SCINTILLATING SCREEN APPLICATIONS IN BEAM DIAGNOSTICS

B. Walasek-Höhne[#], GSI, Darmstadt, Germany
G. Kube, DESY, Hamburg, Germany

Abstract

Scintillating screens are frequently used to detect ionizing particles and are of the great importance for transverse beam profile monitoring at nearly all particle accelerators. The monitor principle relies on the fact that a charged particle crossing the screen material will deposit a part of its energy which is converted into visible light. The resulting photon emission leads to a direct image of the two-dimensional beam distribution and can be measured with standard optical techniques. Simplicity and low cost make this kind of monitor very attractive. In the last years scintillating screen monitors were mainly deployed in hadron and low energy electron machines where the intensity of optical transition radiation (OTR) is rather low. The recent experience from modern LINAC-based light sources shows that even for high energy electron beams standard OTR diagnostics might fail due to coherent effects, thus making the use of scintillators again very attractive. In this paper, a general introduction to the scintillation mechanism in inorganic media will be given. Practical demands and limitations, as well as a brief overview on actual applications at hadron and electron accelerators will be discussed as summary of the "Scintillating Screen Applications in Beam Diagnostics" workshop, recently held in Darmstadt [1].

INTRODUCTION

Inorganic scintillators are widely used for the detection of ionizing radiation. In the past decades significant progress in the discovery of many new scintillator materials and description of the basic physical processes has been made. Reviewing many beam diagnostic applications [2] among the most important properties of a good scintillator are:

- high efficiency in energy conversion into light
- emission spectra matched to the spectral response of the photon detector (e. g. CCD camera)
- high dynamic range and good linearity between the incident particle flux and the light output
- no absorption of emitted light inside the bulk material
- fast decay time for observations of time dependent beam size variations and reduction of saturation effects
- good mechanical and thermal properties
- high radiation hardness to prevent damages

Scintillating screens are a direct intercepting method to observe transverse beam profiles. Profile measurements are important for controlling the spatial distribution of the particle beam, as well as the matching of different sections of the accelerator. In the simplest case (Figure 1), a plate of the scintillating material is inserted into the beam, typically under an angle of 45^0. The screen is observed with a camera system through a viewport, located perpendicular with respect to the beam axis.
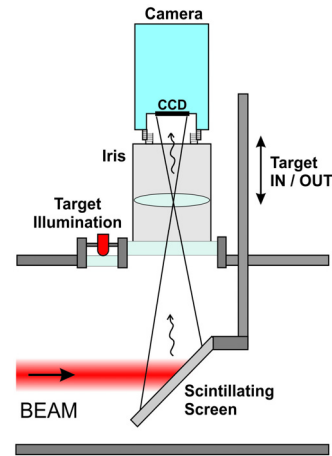

#b.walasek@gsi.de

Figure 1: Scheme of intercepting scintillator screen setup.

SCINTILLATION MECHANISMS

The relaxation of electronic excitations involves complex mechanisms which can be described using a scheme of the electronic band structure of the crystalline scintillator. It includes a core band with top energy E_c, the valence band with top energy $E_v=0$, and the conduction band with bottom energy E_g separated by the band gap. As proposed by Vasil'ev [3], the general time-dependent scheme of scintillation can be described in five main stages as presented in Figure 2. The first stage starts with the production of primary excitations (deep core holes and hot electrons) by interaction of ionizing particles with the material. In a very short time (10^{-16}–10^{-14} s) a large number of secondary electronic excitations is produced by inelastic electron–electron (e–e) scattering and Auger processes with creation of electrons in the conduction band and holes in core and valance bands. This multiplication is stopped when the energy of electrons and holes becomes lower than the threshold of e–e scattering and Auger relaxation, all electrons in the conduction band have an energy smaller than $2E_g$ and all holes occupy the valance band (if there is no core band above the threshold for the Auger process).

The second stage deals with the thermalization of electrons and holes with the production of e.g. phonons. At the end of this stage, all electrons are at the bottom of the conduction band and all holes are at the top of the valence band. In the third stage localization of the excitations through their interaction with stable defects and material impurities can take place. It may occur together with formation of self-trapped excitons (trapping due to lattice relaxation, not attributed to crystalline defects or impurities) and holes in the crystal lattice, the capture of electrons and holes by traps, etc. As a result, these centers have localized states in the band gap. The two last steps are related with migration of relaxed excitations and radiative or/and nonradiative recombination of localized excitations (fourth stage).
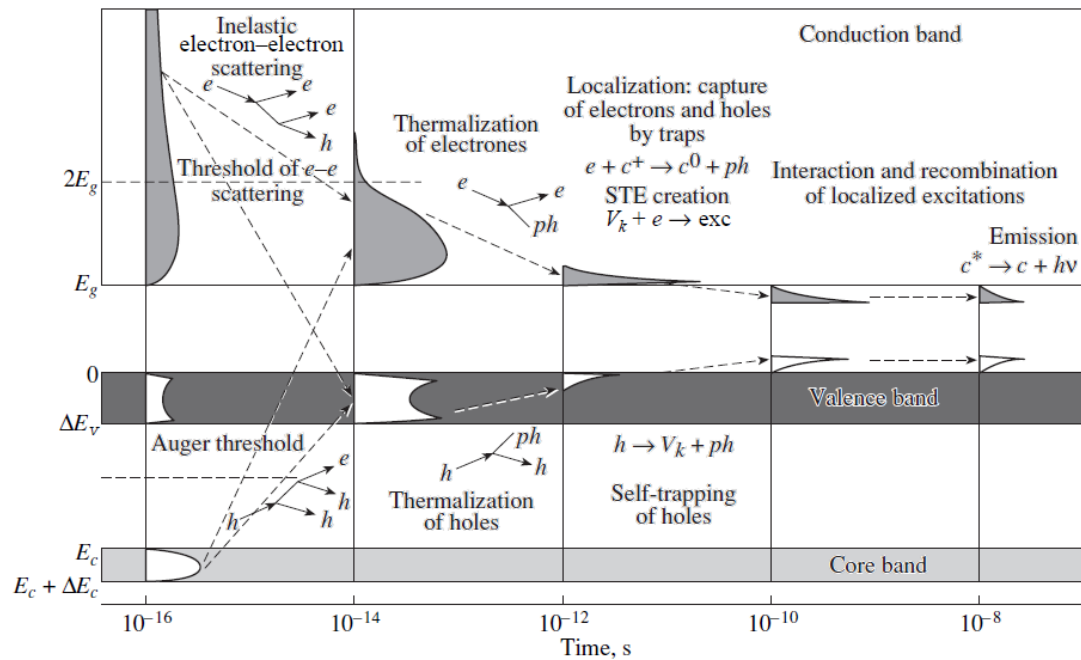
Figure 2: General scheme of relaxation of electronic excitations in an insulating material. It includes five main stages with time scale in abscissa and energy in ordinate [5].

The localization of excitations is sometimes accompanied by a displacement of atoms (defect creation, photo-stimulated desorption) [4]. The fifth stage describes the luminescence of emitting centers excited by the final electronic excitations (correlated electron-hole pairs, excitons, separated electrons, holes, etc.) through sequential capture of charge carriers or various energy transfer processes (luminescence final stage) [4].

In many cases, strong luminescence is obtained by crystals containing rare-earth ions, e.g. Cr based or doped components. The relaxation of electronic excitations involves the 4f band located in the band gap. During the first stage of relaxation, excitation of the rare-earth ions can be obtained through electron impact. The probability of such excitations is significant only when the electron has a kinetic energy below the threshold of e–e scattering and above the threshold of e–rare-earth scattering. So, excited rare-earth centers can be obtained very early. An additional channel of excitation of rare-earth ions is possible after the thermalization stage through sequential capture of holes and electrons by rare-earth ions. The last stage involves radiative combination of luminescent centers of rare-earth centers [5].

Other interesting cases are cross luminescent crystals. Cross luminescence is due to radiative electronic transitions from the valence band to the uppermost core band, providing Auger relaxation of the uppermost core band hole is strictly forbidden. This situation occurs when the energy difference between the uppermost core level and the valence band is smaller than the band gap. The archetype of cross-luminescent crystals is BaF_2 with 5p Ba as an outermost core band which is less than $2E_g$ below the bottom of the conduction band. Such crystals give rise to very short sub-nanosecond luminescence decays, which can be of interest for special applications.

Unfortunately, the light yield is usually relatively weak because only a small number of excitations created in the crystal contribute to cross luminescence [5].

Intraband luminescence is related to radiative transitions between the allowed states either inside the conduction band or in the valence band. The intraband luminescence spectrum is limited by the process of multiplication of electronic excitations, the threshold of which is determined by the value of the ratio energy gap E_g to width of the valance band ΔE_v. As consequence of a high probability of nonradiative transitions between the levels inside the band, the duration of the intraband luminescence is about 1 ps, the spectrum extends over the whole transparency region, and its intensity strongly depends on the width of the band where intraband radiative transitions take place [6]. Fast intraband luminescence is observed e.g. in CsI and MgO. Light output spectrum and decay time are temperature independent (between 7 and 400 K) and not affected by crystal impurities, doping with Na^+ and Tl^+ [7].

SCINTILLATION EFFICIENCY

The scintillation efficiency η can be expressed as the product of three terms:

$$\eta = \beta S Q$$

with β the conversion efficiency for creating electron–hole pairs or excitons, S the transfer efficiency, and Q the radiative efficiency of luminescence centers. Because the energy deposited by a photon or particle E_γ is usually much larger than the band gap E_g of the material, the number of electron–hole pairs and resulting scintillation photons may be very large, thus yielding huge quantum efficiencies. However, the performance of scintillators is less impressive.

For a scintillation photon of energy E_s, this efficiency is given by:

$$\eta\left(\frac{E_s}{E_\gamma}\right) \sim \left(\frac{E_\gamma}{\alpha E_g}\right) SQ\left(\frac{E_s}{E_\gamma}\right) = \left(\frac{E_s}{\alpha E_g}\right) SQ$$

with the assumption that an energy of $\alpha \cdot E_g$ is required to create an electron–hole pair. The factor α can range from about 2 to 7, typical values are 2-3. For materials having transfer and luminescence efficiencies S and Q near unity and a scintillation photon energy approaching the one of the band gap, the energy efficiency should be ~25-30%, which is about the same what has been obtained for the best phosphor materials [8].

Table 1: Room Temperature Efficiencies of Common Inorganic Scintillators [8]

Material	Photons/MeV	Wavelength (nm)	Efficiency (%)
Intrinsic			
CsI	2000	315	0.8
Activated			
CsI:Tl	65000	540	13.7
LSO:Ce	25000	420	7.4
Self activated			
$Bi_4Ge_3O_{12}$	8200	480	2.1

At room temperature, activated components show highest efficiencies as listed in Table 1. For highly efficient scintillators like CsI:Tl (13.7%), the scintillation photon energy is approximately $E_g/2$, therefore S and Q must be close to unity to achieve the measured efficiency.

The efficiency of self activated materials is generally low because Q is reduced due to thermal quenching at room temperature as it is the case for $Bi_4Ge_3O_{12}$ (BGO). The luminescence thermal quenching phenomenon is always related to electron-phonon interactions and non-radiative processes [4]. The light yield of the materials can be increased by operating at lower temperature, but usually at the expense of an increased decay time [8]. Sometimes applications require scintillators with high light output at temperatures higher than room temperatures. Suitable candidates for these applications might be MgO, $LuAlO_3$ or the new inorganic scintillator $Lu_2Si_2O_7$: Ce^{3+} [4].

SCREENS AT HADRON MACHINES

The response of scintillating materials depends on many beam parameters such as energy, intensity, ion species and time structure. Therefore, scintillating materials have to be tailored with respect to specific application demands required at large, universal accelerator facilities. Many investigations described in this paper were performed for particle fluxes much higher than for typical scintillator applications in medical imaging or high energy physics.

Scintillators are ideal to reveal complex structures of the beam (Figure 3, left), but at low energies the deposition of energy and charge in the intercepting material leads to heating problems, electrical charging, and may destroy the screen. Studies at an ion source showed that materials like KBr, quartz glass and BaF_2 have a similar decay rate of the light yield (Figure 3, right), and that the generated light increases linearly with the particle current [9, 10].
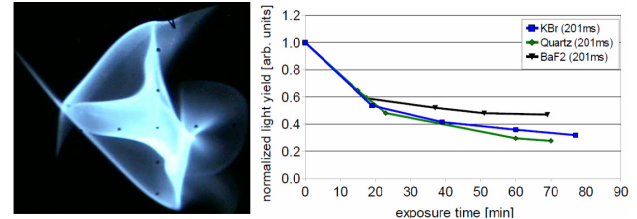

Figure 3: Beam spot behind ion source [9] and light yield versus irradiation time [10].

The studies on sensitivity limits of scintillating screens for beam profile monitoring in the low energy (below 1 MeV/u) and low intensity ($<<10^9$ pps) regime showed that CsI:Tl and Tb glass-based fibre optic plate are sensitive for keV proton beams [11]. As reported in [12], the observed beam profiles change during irradiation, which is a crucial issue for precise measurements. A similar behaviour was observed for several inorganic scintillating materials, during irradiation with high current ion beams at energies below 11.4 MeV/u [13].

Measured properties such as light yield and spot size of the imaged beam profile show a strong dependency on the scintillating material, and change significantly with the screen temperature. The light yield of AlN, ZrO_2:Mg and the quartz glass Herasil® drops significantly with the integrated particle number, but increases slightly for Al_2O_3 [13].
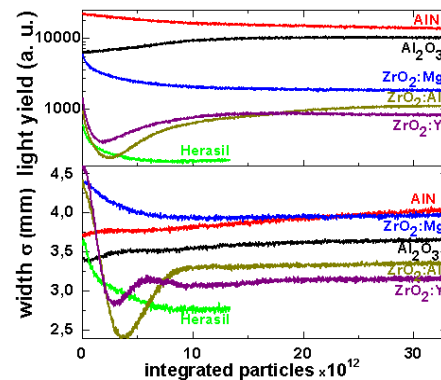

Figure 4: Light yield and beam width versus accumulated ion dose. Beam parameters: Ar^{10+}, $3.3 \cdot 10^{10}$ particles per pulse (ppp) at 11.4 MeV/u and 0.2 ms pulse length [13].

Different materials show different beam readings. For some materials like ZrO_2 doped with Al or Y, the width differs by a factor of two during irradiation (Figure 4). Such behaviour can significantly limit the usability of the monitor. Herasil® shows the smallest beam width, whereas AlN the biggest one [13].

The investigated material properties were also influenced by the temperature as reported in [13, 15].

Visible target modifications were observed after irradiation for most materials, but these modifications do not necessarily imply a lower light yield [13-16].

In addition, spectroscopic studies performed at inorganic scintillators show that damages, generated during intense ion irradiation, can lead to significant changes in the emitted light spectrum. The most prominent change occurs for Herasil® (Figure 5).
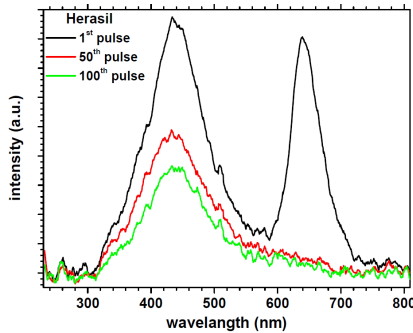

Figure 5: Luminescence spectra of quartz glass Herasil® obtained for the 1st (black), 50th (red) and 100th (green) macro pulse [14].

Detailed studies at GSI for high energy heavy ion beams showed that the light yield of different materials differs by several orders of magnitude and rises almost linearly over a large intensity range (Figure 6). Purpose built scintillators like YAG:Ce and CsI:Tl showed different readings of the imaged beam width compared to P43, ceramic materials, or glasses [17].

Major change of the beam width reading was observed for a Y doped ZrO_2 sample. Similar to the results in [13] also here Herasil® shows the smallest imaged beam width, whereas YAG:Ce shows a broader one.
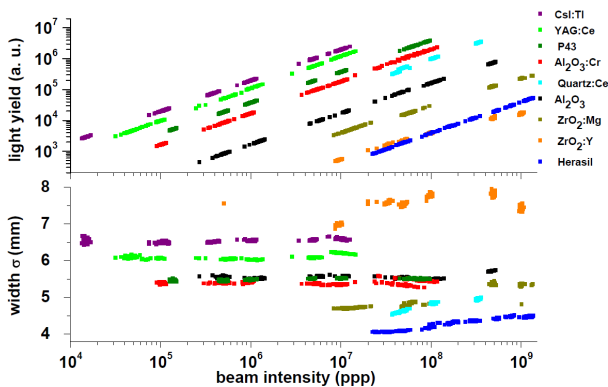

Figure 6: Light yield and beam width as function of beam intensity. Beam parameters: Uranium ions at 300 MeV/u and 300 ms pulse length [17].

SCREENS AT ELECTRON MACHINES

Due to coherent effects in the emission of optical transition radiation (OTR) [18] which may compromise the use of OTR monitors for reliable diagnostics, alternative schemes like the use of luminescent screens are under consideration for modern LINAC-based light sources. Comparison of beam sizes (Figure 7) measured

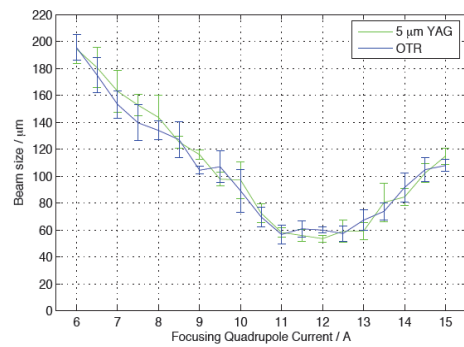with YAG:Ce screens and OTR shows good agreement down to 60 μm rms [19].

Figure 7: Comparison of 200 pC electron beam profiles measured with YAG:Ce and OTR as function of the focusing quadruple current [19].

Studies of different scintillating materials in view of high resolution profile monitoring for high energy and high brilliance electron beams were performed with a micro-focused 855 MeV electron beam [20]. Measured sizes (Figure 8) indicate that LYSO seems to be a suited scintillator material for electron beam profile diagnostics, while the measured beam sizes from the BGO scintillator were slightly larger. It is interesting to note that profiles from the YAG scintillators were significantly larger; similar to the behaviour observed at hadron machines [17]. These results were recently confirmed in a new experiment which is partly described in [21].
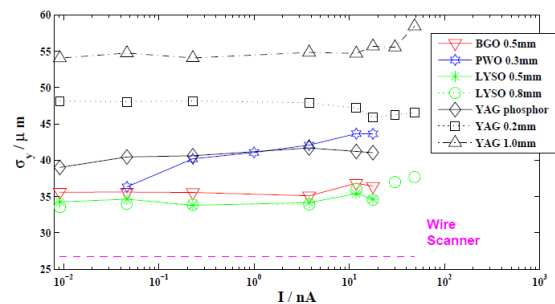

Figure 8: Vertical beam size as function of beam current. The wire scanner measurement was performed only at a beam current of 31 nA [20].

For a micro focused 3.8 nA electron beam, profiles measured with the BGO scintillator were studied as function of the screen rotation angle, thus changing the condition for internal total reflection in the crystal. As can be seen in Figure 9 the measured horizontal beam size exhibits a clear minimum which appears for the orientation when the scintillator surface is tilted away from the CCD surface.

Calculations with ZEMAX® reproduce the general trend in the measured beam sizes quite well. The remaining discrepancy between simulation and measurement seems to be caused by the simplified description of the scintillating light propagation inside the crystal as emission of a line source under pure ray-optical

conditions at the central wavelength of the emission spectrum [20].

Further optical ray-tracing simulations show that the four factors: screen observation angle, scintillator material, scintillating screen thickness, and focal plane can influence the beam profile resolution.
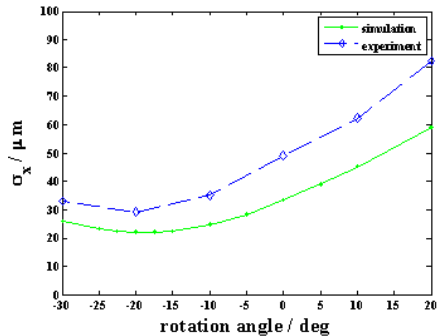

Figure 9: Beam sizes as function of the crystal rotation angle together with the simulation taking into account the internal total reflection [20].

Simulations for different observation angles (90^0, 45^0 and 22.5^0) show that placing a detector under 45^0 with respect to the beam axis offers the best resolution. The refractive index of the scintillating materials can also weakly influence the resolution. The best resolution was achieved for BGO crystal with the biggest refractive index among the three analysed materials (BGO, LuYAP and YAG). Finally, thinner scintillating screens showed better resolution than thicker and the optimum screen tilt angle is not affected by the thickness of the material. The results of this analysis are summarized in [21].

Moreover, the scintillating screen method was proposed and applied to minimize the influence of COTR emission by using a fast gated CCD camera and exploiting the fact that OTR is emitted instantaneously while scintillation light is emitted with a certain decay time [21].

CONCLUSION

The present paper reviews scintillation mechanisms in inorganic media in general case and for three special cases: crystals containing rare-earth, cross luminescence, and intraband luminescence materials.

Recently, there has been significant progress in studies of scintillating screen applications in beam diagnostics. Several detailed investigations on light yield, imaging properties, and spectral response of inorganic scintillators under irradiation with ionizing particles have been performed and showed promising results. It has been demonstrated that the influence of the observation geometry, the scintillating material and scintillator thickness can play an important role in view of high resolution measurements with micro-focused beams.

ACKNOWLEDGEMENT

It is a pleasure to acknowledge many stimulating and informative discussions with the participants of the workshop on "Scintillating Screen Applications in Beam Diagnostics" held in February 2011 in Darmstadt. In particular we would like to thank P. Forck, E. Guetlich, K. Hoehne, P. Lecoq, A. Peters, A. Reiter, M. Schwickert, C. Trautmann, and K. Wittenburg.

REFERENCES

[1] Workshop on "Scintillating Screen Applications in Beam Diagnostics", http://www-bd.gsi.de/ssabd
[2] P. Forck, "Lecture notes on Beam Instrumentation and Diagnostics", Joint Universities Accelerator School (JUAS 2010), http://www-bd.gsi.de
[3] A. N. Vasil'ev, in Proceedings of the 5th International Conference on Inorganic Scintillators and Their Applications, Ed. by V. V. Mikhailin (Moscow State Univ., Moscow, 2000), p. 43
[4] P. Lecoq et al., "Inorganic Scintillators for Detector Systems", Springer
[5] C. Pedrini, "Scintillation mechanisms and limiting factors on each step of relaxation of electronic excitation", Phys. of Solid State, vol. 47, No. 8, 2005
[6] A. Lushchik et al., "Electron and hole intraband luminescence in complex metal oxides", J. of Luminescence, 102-103, 2003
[7] R. G. Deich et al., "Intraband Luminescence in Ionic Crystals", Phys. Stat. Sol., 171, 1992
[8] M. J. Weber., "Inorganic scintillators: today and tomorrow", J. of Luminescence, 100, 2002
[9] J. Maeder, "Usage of viewing screens at the ECR ion source at GSI", Workshop Proceeding, http://www-bd.gsi.de/ssabd
[10] M. Strohmeier, "Scintillator based low energy beam diagnostics at the LBNL 88-inch cyclotron", Workshop Proceeding, http://www-bd.gsi.de/ssabd
[11] J. Harasimowicz et al., "Scintillating screens sensitivity and resolution studies for low energy, low intensity beam diagnostics", Rev. of Scientific Instruments, vol. 81, 2010
[12] G. Perdikakis, "Scintillator screens at ReA3", Workshop Proceeding, http://www-bd.gsi.de/ssabd
[13] E. Guetlich et al., "Scintillation screen investigations for high current ion beams", IEEE Transactions on Nuclear Science, vol. 57, No. 3, (2010)
[14] B. Walasek-Hoehne et al., "Light yield, imaging properties and spectral response of inorganic scintillators under intense ion irradiation", BIW 2010, http://www.JACoW.org
[15] E. Bravin, "Scintillating screens use at CERN", Workshop Proceeding, http://www-bd.gsi.de/ssabd.
[16] U. Raich, "Beam Diagnostics", http://cas.web.cern.ch
[17] P. Forck et al., "Investigation of Scintillation Screens for High Energetic Heavy Ion Beams at GSI", these proceedings, MOPD53
[18] S. Wesch, B. Schmidt, "Summary of COTR effects", these proceedings, WEOA01
[19] R. Ischebeck, "Scintillators for SwissFEL", Workshop Proceeding, http://www-bd.gsi.de/ssabd
[20] G. Kube et al., "Resolution Studies on Inorganic Scintillation Screens for High Energy and High Brilliance Electron Beams", IPAC 2010
[21] M. Yan et al., "Suppression of COTR in Transverse Beam Diagnostics by Utilizing a Scintillation Screen in Combination with a Fast Gated CCD Camera", these proceedings, TUPD59